A scientist counts calories to make sense of human evolution p. 710

Ordinary bilayer graphene is superconducting pp. 719 & 774

New insights on the peopling of the Americas p. 727

Science

$15
18 FEBRUARY 2022
science.org

AAAS

QUICK RELEASE

How lizards rapidly shed their tails to escape predators pp. 721 & 770

BIOMECHANICS

Biomimetic fracture model of lizard tail autotomy

Navajit S Baban[1], Ajymurat Orozaliev[1], Sebastian Kirchhof[2], Christopher J Stubbs[3], Yong-Ak Song[1,4,5]*

Lizard tail autotomy is an antipredator strategy consisting of sturdy attachment at regular times but quick detachment during need. We propose a biomimetic fracture model of lizard tail autotomy using multiscale hierarchical structures. The structures consist of uniformly distributed micropillars with nanoporous tops, which recapitulate the high-density mushroom-shaped microstructures found on the lizard tail's muscle fracture plane. The biomimetic experiments showed adhesion enhancement when combining nanoporous interfacial surfaces with flexible micropillars in tensile and peel modes. The fracture modeling identified micro- and nanostructure-based toughening mechanisms as the critical factor. Under wet conditions, capillarity-assisted energy dissipation pertaining to liquid-filled microgaps and nanopores further increased the adhesion performance. This research presents insights on lizard tail autotomy and provides new biomimetic ideas to solve adhesion problems.

For millions of years, the constant struggle for survival has driven lizards to evolve a defense mechanism known as tail or caudal autotomy (*1*, *2*). This autotomy has a seemingly paradoxical nature: sturdy attachment at normal times but quick detachment during need. As an explanation of tail autotomy, previous studies have reported the segmented anatomy of the lizard tail with functional fracture planes (*3*, *4*) in skeletal muscles throughout the postpygal vertebrae (for details, see supplementary text 1). The fracture planes consist of the bulged-out distal ends of muscle fibers arranged as highly dense, mushroom-shaped micropillars (separated by connective tissue) (*3*, *4*) with a role in autotomy that is still not understood quantitatively.

From an engineering perspective, a typical fracture plane would make the tail overly vulnerable to fracture, even in situations that are not life threatening. In reality, the tail remains sturdily and faithfully connected to the body part, quickly detaching only when the lizard wills it. Simplistic fracture models of lizard tail autotomy cannot resolve the tail's attachment's seemingly paradoxical nature. A proteomic study (*3*) on the fluid that was released after Tokay gecko tail autotomy revealed an absence of any protein-breaking chemicals, thus suggesting a mechanical fracture problem. To understand the biophysics of lizard tail autotomy, we analyzed the fracture plane connections of three different lizard species: *Hemidactylus flaviviridis* (Gekkonidae), *Cyrtopodion scabrum* (Gekkonidae), and *Acanthodactylus schmidti* (Lacertidae).

Fig. 1A shows the autotomy location in the *H. flaviviridis* individual's tail and illustrates the segmented nature of the tail connected

[1]Division of Engineering, New York University Abu Dhabi, Abu Dhabi, United Arab Emirates. [2]Division of Science, New York University Abu Dhabi, Abu Dhabi, United Arab Emirates. [3]Gildart Haase School of Computer Sciences and Engineering, Fairleigh Dickinson University, Teaneck, NJ 07666, USA. [4]Department of Chemical and Biomolecular Engineering, Tandon School of Engineering, New York University, New York, NY 11201, USA. [5]Department of Biomedical Engineering, Tandon School of Engineering, New York University, New York, NY 11201, USA.
*Corresponding author. Email: rafael.song@nyu.edu

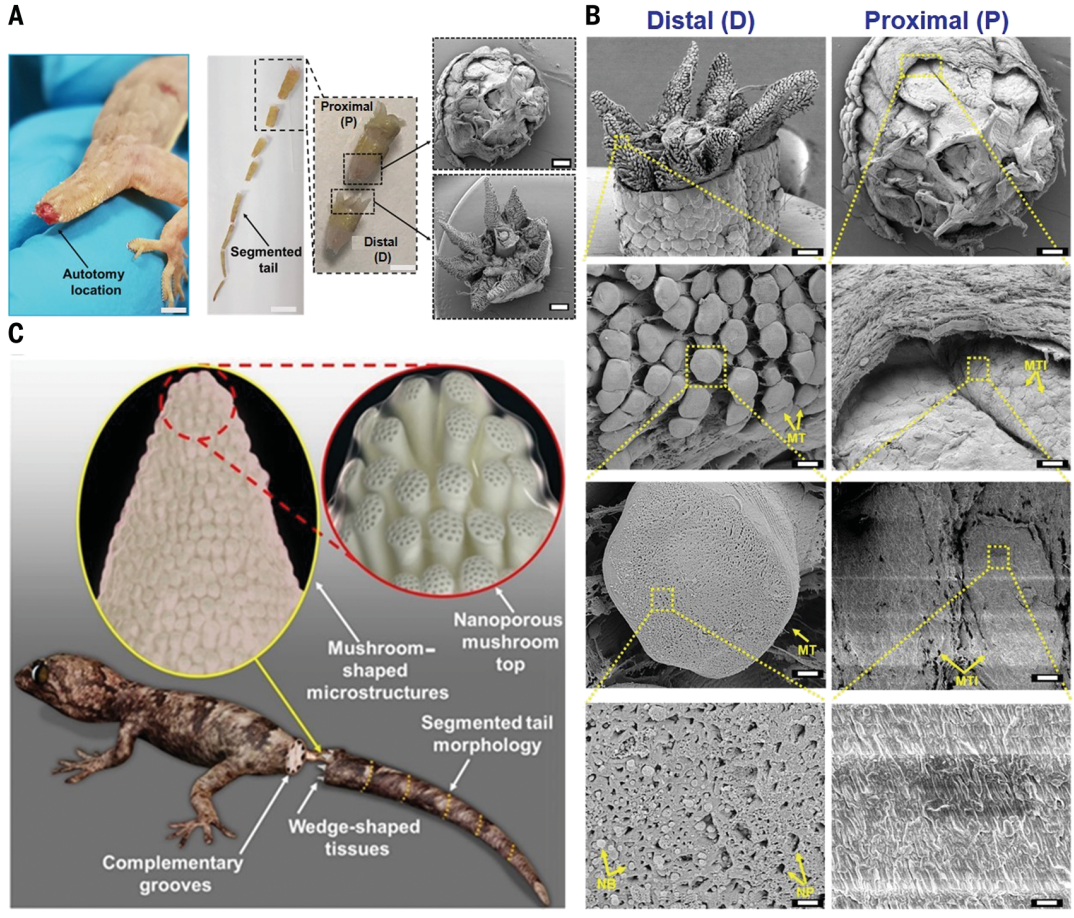

Fig. 1. Scanning electron microscope (SEM) image of the autotomized interface of an *H. flaviviridis* tail. (**A**) Autotomized tail location (scale bar, 1.5 cm). Segmented tail morphology (scale bar, 1 cm) shows region P, representing the proximal part of the tail, and region D, representing the distal part (scale bar, 0.5 cm), in a plug-and-socket type assembly (scale bar, 1 mm). (**B**) SEM of the distal (D) part showing the wedge-shaped tissues with highly dense mushroom-shaped microstructures (scale bar, 1 mm). The enlarged portion shows the mushroom-shaped micropillared arrangement (scale bar, 100 μm) with the single mushroom top indicated as MT (scale bar, 10 μm) containing the nanopores (NP) and nanobeads (NB) (scale bar, 1 μm). SEM of region P (scale bar, 1 mm) shows the corresponding MT imprints indicated as MTI (scale bar, 100 μm). The single MTI (scale bar, 10 μm) shows a planar topology (scale bar, 1 μm). (**C**) Hypothesized model of the lizard tail interface between two complementary segments before fracture, consisting of micropillared nanoporous top connections at the wedge-shaped tissue faces.

Downloaded from https://www.science.org at New York University on February 18, 2022

through a "plug-and-socket" sort assembly. The distal part contains eight (two ventral, four lateral, and two dorsal) circumferentially arranged wedge-shaped muscle bundles, whereas the proximal part encloses the corresponding complementary grooves or pockets lined with layers of connective tissue (myosepta). Fig. 1B shows the high-density mushroom-shaped micropillars (muscle fibers with dilated termini) on the wedge-shaped muscle bundle and the complementary pockets where the wedges remained inserted before fracture. Microcomputer tomography of the fractured tail (*H. flaviviridis* individual) showed fragmented intravertebral fracture planes located in close proximity to the wedge-shaped muscle fracture planes (see supplementary text 2). The enlarged portions within Fig. 1B show the associated mushroom top with dense nanopores and scanty nanobeads constituting the interface. The magnified view of the complementary pockets shows the planar mushroom top imprints in the myoseptum resulting from its surface contact–based attachment with the mushroom top in vivo. These surface imprints implied that the mushroom tops were not penetrating the proximal part, as would be the case for stronger tail attachment. Instead, the lizard has adopted a different strategy for tail attachment at the interface composed of the surface contact–based attachment with microscale and nanoscale discontinuities. Thus, we hypothesize a model of how the distal tail section could have been attached to the proximal one before fracture, in which mushroom-shaped microstructures contact the opposite surface with their nanoporous tops, as schematically illustrated in Fig. 1C.

These multiscale hierarchical features correlated with design strategies extensively found in nature (for examples, see supplementary text 3) that imply toughening mechanisms associated with micro- and nanoscale structural features. The high-speed video analysis showed that the tail's bending actuated the fracture (movies S3 and S4 and supplementary text 4). By contrast, the tensile stretching of the tail showed no fracture at all (Fig. 2). Moreover, on the basis of the *H. flaviviridis* specimens analyzed (n = 7), it was also confirmed that the tail should be grasped at least a short distance distal to the autotomy plane. This would provide a sufficient pivot length about which the muscles can favorably act. For *A. schmidti*, the shorter pivot distance required more force to induce the fracture (movie S5 and S6).

To support our hypothesis, we built a biomimetic model using polydimethylsiloxane micropillars with nanoporous tops in two different height ranges: 1.75 to 30 μm as low-aspect-ratio micropillars and 30 to 100 μm as high-aspect-ratio micropillars (Fig. 3, A and B). For both the low- and high-aspect-ratio micropillars, the results in Fig. 3, C to H and I to N (summarized in table S1), show that adhesion energy and peak force significantly decreased in peel mode (see experimental details in supplementary text 5), demonstrating the fracture's mode-dependent vulnerability. The difference in mode-dependent results can be explained by the equal load sharing of the micropillars (*5*), which was quantified by comparing the associated characteristic stress decay lengths (*6*, *7*). We recorded a 17-fold difference between the modes (see the "Equal load sharing calculation" section in supplementary text 5). The mode-dependent findings correlated with the experimental results of the high-speed video analysis showing a facile fracture in the bending mode.

Within each mode, a significant increase in adhesion energy and peak force was obtained at nanoporous top surfaces, thus validating the role of micropillared nanoporous interface in improving the adhesion performance. The combined use of micropillared interface with nanoporous top showed a significant adhesion enhancement for both low-aspect ratio micropillars (maximally, 7.9-fold in the tensile mode and 4.5-fold in the peel mode) and high-aspect ratio micropillars (maximally, 14.8-fold in the tensile mode and 14-fold in the peel mode) compared with the plain unstructured interface. The enhancement effect of the nanoporous interface can specifically be filtered out by comparing the plain top and nanoporous top pillars' results, in which a significant adhesion increment was recorded for both the low-aspect-ratio micropillar (4.8-fold in the tensile mode and 2.5-fold in the peel mode) and the high-aspect-ratio micropillar (1.4-fold in the tensile mode and 2.1-fold in the peel mode).

The hierarchical toughening can be explained as follows. First, the nanoporous-assisted contact on top of the micropillars exerts a crack-arresting effect that can be explained by the crack initiation at multiple discontinuities plus the coplanar Cook-Gordon mechanism (*7*, *8*) that imparted repulsive stress interactions between the vicinal coplanar cracks (*8*, *9*) during propagation. This greatly contributed toward the intrinsic (*10*) fracture toughening mechanism at the interface. Furthermore, multiple nanolevel discontinuity-associated intermittent crack propagations induced a coplanar Lake-Thomas (*8*) effect that dissipated energy similar to bond rupturing in soft elastomer chains. Second, the phenomenon of flaw insensitiveness (*5*) caused by micropillar-based contact-splitting phenomena also contributed to the increasing adhesion through extrinsic (*10*) toughening in tandem with the nanopore-induced intrinsic toughening. Last, as the micropillars' height increased, a considerably large amount of strain energy was absorbed by the flexible micropillars, improving the extrinsic toughening further (see the "Flaw insensitivity" and "Effect of micropillar height" sections in supplementary text 5). For the high-aspect-ratio micropillars, the 100-μm-high micropillars that closely resembled the mushroom-like microstructures in terms of their aspect ratio showed the highest adhesion energy and peak forces.

We also evaluated the effect of strain rate, prestress, and wet conditions (see supplementary text 6) and found improvement in adhesion performance in all cases. The adhesion performance improvement in wet conditions was attributed to the combined effect of microscale and nanoscale liquid bridges (*11*) in dissipating elastic energy, plus the spatially varying

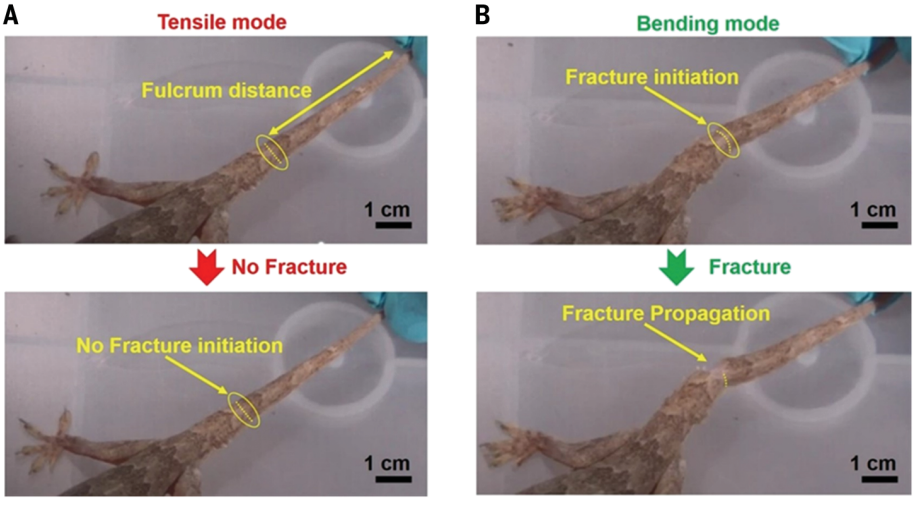

Fig. 2. High-speed analysis of tail autotomy. (**A**) Tensile mode, in which the tail was in the fully stretched condition with the fulcrum distance between the fracture plane and the grasp point. No fracture initiation was observed for the tensile stretching mode. (**B**) Bending mode, in which the tail was in the fully stretched condition showing fracture initiation. Catastrophic fracture propagation was observed after the fracture initiation in the bending mode.

Downloaded from https://www.science.org at New York University on February 18, 2022

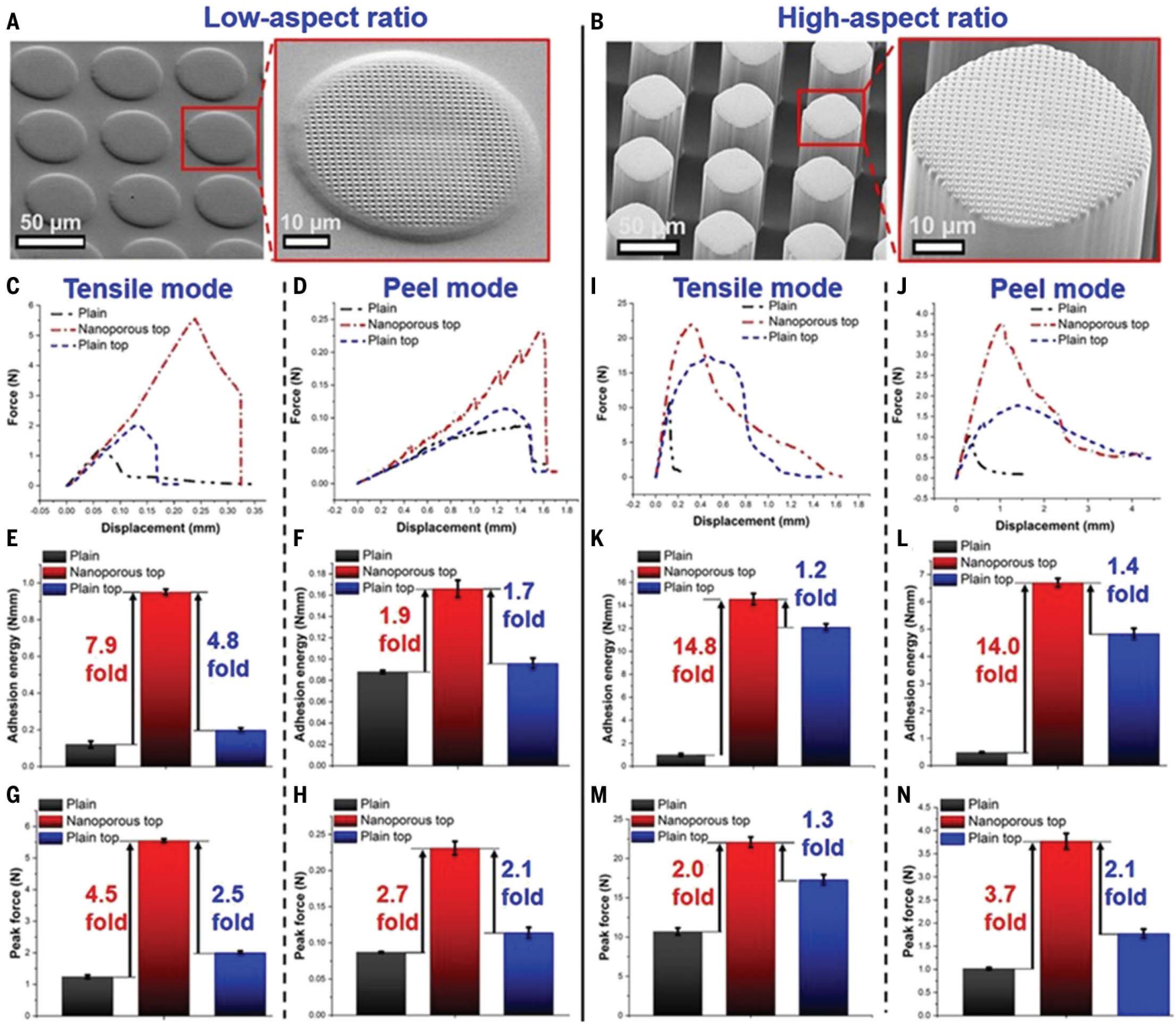

Fig. 3. Adhesion test results using a biomimetic model. (**A**) Low-aspect-ratio nanoporous top micropillars (50 μm in diameter, 1.75 μm in height). (**B**) High-aspect-ratio nanoporous top micropillars (50 μm in diameter, 100 μm in height). (**C** to **H**) Results for the low-aspect-ratio micropillars. Shown are force-displacement curves [(C) and (D)], adhesion energy results [(E) and (F)], and peak force results [(G) and (H)]. (**I** to **N**) Results for the high-aspect-ratio micropillars. Shown are force-displacement curves of the fracture tests [(I) and (J)], adhesion energy results [(K) and (L)], and peak force results [(M) and (N)]. The sample number was $n = 10$ for each case. The error bars represent SD. Each difference in the figure was significant with a P value < 0.05.

modulus during contact separation (*12*). Regarding the prestress condition at the interface before fracture, we found a notable effect of the prestress in restricting the fracture initiation and propagation. On the basis of this finding, we hypothesize that relieving the prestress by the skeletal muscle fibers' contraction (*4*) would provide favorable autotomy conditions.

To analyze and compare the toughening mechanism at the nanoscale and microscale levels, we also performed cohesive zone modeling and submodeling (*7*). The contour plots in Fig. 4 show the repulsive (*9*) stress interaction between the primary and the secondary crack, which was generated because of the subsequent nanopore-induced discontinuity (supplementary text 7). The plain top micropillar interface in Fig. 4, A and B, showed a single crack front with a larger crack tip stress singularity zone compared with the nanoporous top in both the tensile mode (Fig. 4, C and E) and the peel mode (Fig. 4, D and F). The stresses were distributed through nanolevel discontinuities, indicating intermittent crack propagation [as described in the coplanar version of the Lake-Thomas effect (*8*)], with considerably less crack tip singularity. Fig. 4, G and H, compare the strain energy dissipation or release rate and contact opening between the nanoporous and plain top pillar interface. A decrease in the strain energy release rate was found between the concerned interfaces (54 and 48% for the tensile and peel modes, respectively). Similarly, a decrease in the contact opening was found between the concerned interfaces (19 and 39% for the tensile and peel modes, respectively), illustrating the nanoporous interface's intrinsic toughening effect.

Our studies based on two species of the Gekkonidae and one species of the Lacertidae lizard family revealed an essential role of the highly dense mushroom-shaped micropillars

Downloaded from https://www.science.org at New York University on February 18, 2022

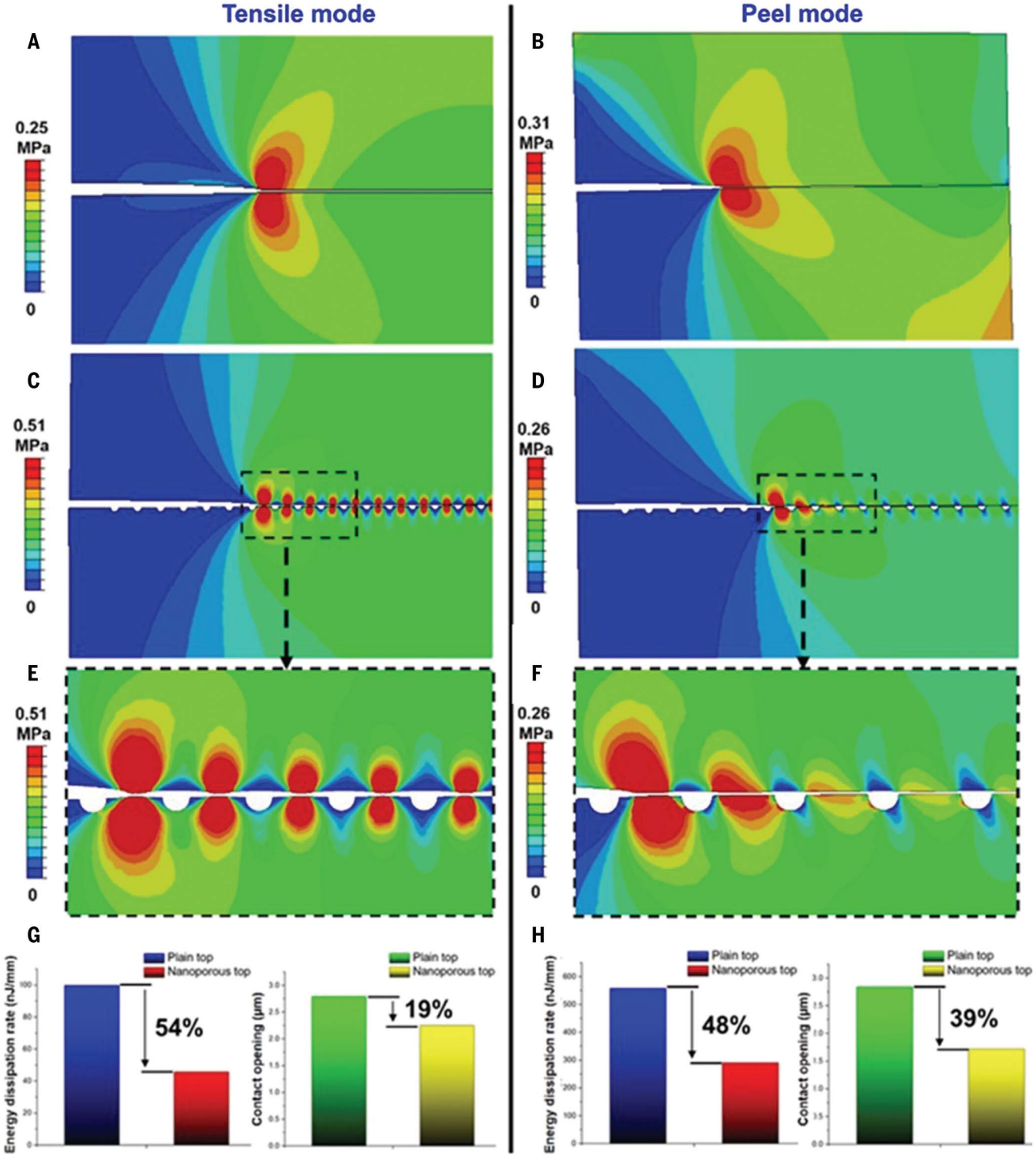

Fig. 4. Computational fracture modeling of a plain top versus nanoporous micropillar interface. (**A** to **D**) Maximum principal stress contour plots for the plain top micropillar (1.75 μm in height) in the tensile mode (A) and in the peel mode (B) and for the nanoporous top micropillar in the tensile mode (C) and in the peel mode (D). (**E** and **F**) Stress field interaction as a result of the coplanar Cook-Gordon mechanism in the tensile mode (E) and in the peel mode (F). (**G** and **H**) Strain energy dissipation rate and contact opening comparison in the tensile mode (G) and in the peel mode (H).

with nanoporous top surfaces in tail autotomy. These micropillars and nanopores establish interfacial connections along the tail fracture planes that are exposed to higher vulnerability in bending mode than in tensile mode. However, within each mode, the connections showed toughening mechanisms with nanoporous top micropillars that helped the tail avoid undue breakage. The intrinsic toughening mechanisms were composed of nanolevel crack discontinuities that assisted the coplanar version of the Cook-Gordon mechanism and the Lake-Thomas effect. Furthermore, the increased height of micropillars, as well as the flaw insensitivity caused by microlevel discontinuities, contributed

Downloaded from https://www.science.org at New York University on February 18, 2022

to the extrinsic toughening mechanisms. In wet conditions, microscale and nanoscale liquid bridges facilitated capillary-assisted and suction-based energy dissipation. This, along with the toughening mechanisms associated with direct solid-solid contact, improved the adhesion performance. Using this multiscale interfacial strategy, the lizard carefully balances attachment and detachment, achieving the "just right" connection in its tail that is neither too weak nor too strong for its best chance of survival.

REFERENCES AND NOTES

1. E. N. N. Arnold, *J. Nat. Hist.* **18**, 127–169 (1984).
2. P. W. Bateman, P. A. Fleming, *J. Zool.* **277**, 1–14 (2009).
3. K. W. Sanggaard *et al*., *PLOS ONE* **7**, e51803 (2012).
4. T. H. Araújo, F. P. de Faria, E. Katchburian, E. F. Haapalainen, *Acta Zool.* **91**, 440–446 (2010).
5. A. Jagota, C. Y. Hui, *Mater. Sci. Eng. Rep.* **72**, 253–292 (2011).
6. D. A. Dillard, B. Mukherjee, P. Karnal, R. C. Batra, J. Frechette, *Soft Matter* **14**, 3669–3683 (2018).
7. N. S. Baban, A. Orozaliev, C. J. Stubbs, Y. A. Song, *Phys. Rev. E* **102**, 012801 (2020).
8. J. Y. Chung, M. K. Chaudhury, *J. R. Soc. Interface* **2**, 55–61 (2005).
9. J. C. Hill *et al*., *Int. J. Fract.* **119**, 365–386 (2003).
10. R. O. Ritchie, *Nat. Mater.* **10**, 817–822 (2011).
11. Q. Liu *et al*., *ACS Appl. Mater. Interfaces* **12**, 19116–19122 (2020).
12. A. Ghatak, *Phys. Rev. E Stat. Nonlin. Soft Matter Phys.* **89**, 032407 (2014).

ACKNOWLEDGMENTS

We thank A. Bauer for helpful discussions on the biology of tail autotomy; P. Salmon from Bruker Belgium for CT scanning the lizard tail; the NYU Abu Dhabi graduate office for providing N.S.B. with a Global Ph.D. Fellowship; and the NYU Abu Dhabi Core Technology Platform, especially R. Pasricha and J. Weston, for providing us access and help with the SEM study. **Funding:** This work was supported by an annual research grant provided by NYU Abu Dhabi. **Author contribution:** N.S.B. conducted SEM analysis, high-speed videography and analysis, biomimetic sample preparation, characterization and results analysis, and finite element simulations. A.O. fabricated masters for the biomimetic model. S.K. was in charge of lizard biology and evolution and assisted in capturing, identifying, and performing high-speed videography of autotomy. C.J.S assisted and checked finite element simulations. Y.A.S planned, guided, and coordinated the project. All authors contributed to the writing of the manuscript. **Competing interests:** The authors declare no competing interests. S.K is also affiliated with the Museum für Naturkunde Berlin, Leibniz Institute for Evolution and Biodiversity Science, Berlin (Germany) as a guest researcher, but this affiliation has no competing interests for the current paper. **Data and materials availability:** All data and materials are available in the main manuscript or the supplementary materials.

SUPPLEMENTARY MATERIALS

science.org/doi/10.1126/science.abh1614
Materials and Methods
Supplementary Text 1 to 7
Figs. S1 to S32
Tables S1 to S4
References (*13*–*31*)
Movies S1 to S12

Accepted 20 December 2021

21 February 2021; resubmitted 5 November 2021
Accepted 20 December 2021
10.1126/science.abh1614

Downloaded from https://www.science.org at New York University on February 18, 2022

Science

Biomimetic fracture model of lizard tail autotomy

Navajit S BabanAjymurat OrozalievSebastian KirchhofChristopher J StubbsYong-Ak Song

Science, 375 (6582), • DOI: 10.1126/science.abh1614

Engineered for a quick escape

When under attack, lizards will shed their tails as a way of escaping the predator while leaving behind a wiggling decoy to distract the enemy. The tail needs to be firmly attached most of the time, but it must also have a quick-release mechanism that won't engage during normal activities. Baban *et al.* devised a multiscale hierarchical model for the tail attachment (see the Perspective by Ghatak). Microscopy data of the broken surfaces of the tail showed that the fracture plane consists of mushroom-shaped pillars with nanopores at their tops. These pillars allow for enhanced adhesion of the tail in tension and peeling modes but enable fracture during oscillatory bending. The authors confirmed their hypothesis using polymer models and modeling. —MSL

View the article online
https://www.science.org/doi/10.1126/science.abh1614
Permissions
https://www.science.org/help/reprints-and-permissions

Downloaded from https://www.science.org at New York University on February 18, 2022

Use of think article is subject to the Terms of service

Science (ISSN) is published by the American Association for the Advancement of Science. 1200 New York Avenue NW, Washington, DC 20005. The title *Science* is a registered trademark of AAAS.
Copyright © 2022 The Authors, some rights reserved; exclusive licensee American Association for the Advancement of Science. No claim to original U.S. Government Works

opment could lead to permanent damage to neurological function (*5*). The biological mechanisms of how EDCs influence human fetal brain development are difficult to study, partly because the tools to effectively monitor brain development in utero are lacking (*7*).

Standard chemical risk assessment consists of several steps, including quantification of chemical exposure for a given population (exposure assessment), determination of safe concentrations for chemicals (hazard identification and characterization), and estimation of the health risks associated with exposures (risk characterization) (*8*). Over the past 60 years, chemical risk assessments for thousands of individual environmental substances have been performed. Regulatory agencies have now started to develop guidelines to assess chemical mixtures (*9*).

Caporale *et al.* used a population-based cohort of 1874 mother-child pairs enrolled from Sweden during 2007–2010 with measured concentrations of PFASs, phthalates, bisphenol A, and triclosan in serum or urine from mothers in the 10th week of pregnancy. They estimated an EDC mixture that was associated with subsequent delayed language development in children using biostatistical modeling. About 10% of children in the cohort had language delay, defined as the use of fewer than 50 words at the age of 30 months old. Six varying concentrations of the EDC mixture identified from this cohort analysis were tested in multiple experimental models, including human cerebral organoids, *Xenopus laevis* tadpoles, and zebrafish larvae. The authors identified gene networks altered by the EDC mixture in human cerebral organoids, and validated thyroid, estrogen, and peroxisome proliferator-activated receptor (PPAR) endocrine pathways as major convergent targets in vivo. Based on these empirical data, the authors estimated that ~54% of the children in the cohort had been prenatally exposed to EDC mixture concentrations that could induce biological effects, including language development.

The traditional risk assessment approach depends on testing single chemicals across dosage concentrations in animal models, but uncertainty remains about directly applying these toxicological outputs to guide policy. This is especially true when testing a combination of chemicals; there are multitudinous combinations (in terms of relative proportions and concentrations) between and within different classes of chemicals to consider. Caporale *et al.* showed that the existing human epidemiological cohort data can be used to guide and determine typical human-relevant mixtures and subsequently test their biologic and molecular effects in relevant in vitro and in vivo models. This integrated approach strengthens the causality of the exposure-outcome associations observed in human cohorts and improves the generalizability of experimental data.

The success of this approach, however, is highly dependent on the mixture analysis from the cohort study to be valid. Methodological challenges in environmental epidemiological research—such as errors in measuring exposures or health outcomes, uncontrolled confounding or selection bias, and incorrect statistical models—could threaten the validity of findings. Multiple experiments were conducted by Caporale *et al.*, but drawing conclusions might have become difficult if the results from each did not collaborate. The extent to which and how many such experiments are needed to generate reliable data for mixture risk assessment is unclear.

The study of Caporale *et al.* focused on three classes of EDCs, but this is not an exhaustive list of chemicals of concern. For example, it has been reported that more than 4000 PFASs have been applied in commercial products, whereas, at present, no human studies can accurately detect and quantify the concentrations for all possible PFASs (*6*). Technological advancement and cost-effective methods are needed to generate exposure profiles accurately and comprehensively. Setting up a longitudinal cohort study is costly and time consuming. A continuing investment to support ongoing cohorts (to assess cumulative exposure and long-term health impacts) as well as setting up new cohorts (to capture contemporary exposure profiles) is essential to keep up with assessing and mitigating human exposure to harmful chemical mixtures. A framework is also needed for mixture risk assessment to test new chemicals (including the replacement of recently banned chemicals) that are rapidly introduced in the global environment. ■

REFERENCES AND NOTES

1. M. A. La Merrill *et al.*, *Nat. Rev. Endocrinol.* **16**, 45 (2020).
2. N. Caporale *et al.*, *Science* **375**, eabe8244 (2022).
3. G. W. Olsen *et al.*, *Environ. Health Perspect.* **115**, 1298 (2007).
4. L. G. Kahn *et al.*, *Lancet Diabetes Endocrinol.* **8**, 703 (2020).
5. T. Colborn *et al.*, *Our Stolen Future: Are We Threatening Our Fertility, Intelligence, and Survival? A Scientific Detective Story* (Plume, 1996).
6. E. M. Sunderland *et al.*, *J. Expo. Sci. Environ. Epidemiol.* **29**, 131 (2019).
7. L. Konkel, *Environ. Health Perspect.* **126**, 112001 (2018).
8. R. Eisler, *Handbook of Chemical Risk Assessment: Health Hazards to Humans, Plants, and Animals* (CRC Press, 2000).
9. E. S. Committee *et al.*, *EFSA J.* **17**, e05634 (2019).

ACKNOWLEDGMENTS

Z.L. is supported by the National Institutes of Health–National Institute of Environmental Health Sciences Pathway to Independence Award (R00ES026729).

10.1126/science.abn9080

[1]Department of Environmental Health Sciences, Yale School of Public Health, Yale University, New Haven, CT, USA. [2]Yale Center for Perinatal, Pediatric, and Environmental Epidemiology, Yale School of Public Health, New Haven, CT, USA. Email: zeyan.liew@yale.edu

BIOPHYSICS

How does a lizard shed its tail?

Hierarchical microstructures help a lizard self-amputate its tail when needed

By **Animangsu Ghatak**

Among many escape strategies that animals have evolved to evade capture by their predators, autotomy is a prominent one, whereby an animal self-amputates a body part, such as a leg or a tail (see the photo), just to elude its attacker. The ease with which animals can shed their body parts depends on the anatomy of the joint that connects the said body part to their body (*1*). How does the animal ensure that a limb does not shed off during its regular activity yet easily and quickly detaches when it struggles to escape the grasp of a predator? On page 770 of this issue, Baban *et al.* (*2*) show that for lizards that self-amputate their tail when under threat, the hierarchical microstructure of the tail plays an important role in this balancing act.

The lizard tail consists of segments separated by distinct fracture planes that are weak zones. Experiments with three different lizard species—*Hemidactylus flaviviridis*, *Cyrtopodion scabrum*, and *Acanthodactylus schmidti*—show that these planes are not smooth but instead consist of microscopic structural features with sizes spanning from hundreds of micrometers down to tens of nanometers. On the larger side, the tail consists of a wedge-shaped tissue assembly, the proximal and distal parts of which form a "plug and socket" type of arrangement. Going down to the submillimeter scale, the tissue surface contains microscopic pillars in the shape of mushrooms. Zooming in even further, the "mushroom heads" themselves are decorated with nanoscopic pores and, in some cases, nanoscopic beads. Proteomic studies and scanning electron microscopy of the fractured planes show that the mushrooms that compose the cleaved surface of the tail do not get into mechanical interlocking or covalent

Department of Chemical Engineering, Indian Institute of Technology Kanpur, Kanpur, Uttar Pradesh, India. Email: aghatak@iitk.ac.in

Downloaded from https://www.science.org at New York University on February 18, 2022

Researchers have shown that caudal autotomy in lizards, such as that seen in the Japanese five-lined skink (*Eumeces japonicus*) pictured here, is mediated by the hierarchical microstructures at the fracture plane of their tails.

bonding with the main body of the animal but rather form physical bonds through adhesive forces.

Baban *et al.* show that this adhesion is strong enough that the tail does not break away during regular activities. Indeed, straight pulling of the tail does not result in any failure at all. On the contrary, when a supposed predator grabs the tail a small distance down a fracture plane, a slight act of bending of the tail initiates a crack from one side, which propagates catastrophically and leads to complete separation of the portion of the tail that is under siege. It seems that hierarchy in microstructure helps the tail by providing flexibility to the mushroom-shaped structures present on the fractured surface of the severed limb. This flexibility allows these structures to remain in intimate contact with the complementary surface of the animal's body. The mushrooms help distribute the pulling load throughout the area of contact. As a result, the magnitude of stresses at the interface hardly gets large enough to cause a separation. Structural hierarchy also generates spatial modulation in topography as well as variation in deformability, features that help to trap and deflect a crack. A trapped crack loses all its energy to propagate forward and gets reinitiated only when the interface is sufficiently stretched again at the location of the crack tip. In wet conditions, liquid nanobridges between the contacting surfaces increase adhesion further through capillary forces.

The findings of Baban *et al.* are relevant to similar hierarchical features that are present on the feet of many wall-climbing animals (*3*–*6*). Geckos, insects, and frogs have all drawn the attention of scientists for their exceptional ability to walk or dart on a variety of surfaces in their habitat, often when situated on a vertical surface or even completely upside down. The strong, yet reversible, adhesion at their feet is derived from hierarchical microstructures that divide into finer and finer hairs, which terminate as spatula- or mushroom-shaped caps (*7*). Billions of these hairs or bristles not only allow these animals to follow the contours of the nano- to microscopic roughness of the surface that they hold on to but also help in debonding and reattaching through multiple crack arrests and reinitiation at the edge of each of these caps (*8*).

Subsurface effects, like tunable pressure within sacs filled with liquid or air (*4*, *9*) and hysteretic adhesion at the internal walls of subsurface vessels, further amplify the effect of crack arrest (*10*, *11*) and the consequent dissipation of energy. In some cases, a liquid emerges from tiny holes on the bristles to form a capillary bridge with the adherent surface, resulting in both strong and switchable adhesion. (*12*, *13*). When the animal's foot is pulled off perpendicular to the surface, hundreds and thousands of minuscule attachments distribute the load and help resist separation. By contrast, during bending or peeling from one edge of the contact, the pulling stress gets sufficiently concentrated at the peeling front so that the crack can overcome the resistance to fracture, similar to the mechanism of autotomy of the lizard tail.

The findings of Baban *et al.* are quite notable in that a phenomenon such as self-amputation, which was previously believed to occur through a cohesive fracture, is shown to be the result of adhesive failure mediated by physical principles linked to the structural hierarchy of the adherent surfaces. It is worth noting that not only lizards, but also salamanders, crustaceans, spiders, mice, and worms, use autotomy as a defense strategy, and it will be interesting to determine whether these animals use adhesion as the dominant mechanism for keeping their expendable limb connected to the main torso.

Autotomy is but one strategy that organisms have evolved to escape capture by their predators. However, it starkly contrasts other survival skills that work either on the principle of camouflage or on the ploy of a preemptive strike, such as spraying hot and toxic chemicals or oozing out a bad odor (*14*). Yet a large variety of species in the animal kingdom and even some plant species use autotomy to survive. For example, plants like sourgrass resort to autotomy (*15*) for defending themselves from being completely uprooted when pulled by herbivores. A notch present at the base of the stalk of the leaves of these plants acts as a weak link that ensures that only the leaf gets torn away, thereby saving the whole plant. Thus, autotomy proves to be a successful survival tool in the natural world, and its prevalence in both plants and animals gives confidence that it may be useful for scientific and engineering applications. Particularly in robotics, stealth technology, and prosthetics and for the safe operation of many critical installations, an optimized link similar to the one present at the lizard tail can go a long way in protecting an expensive component or a device from an unforeseen accident or mishap. ■

REFERENCES AND NOTES

1. I. Fernández-Rodríguez, F. Braña, *J. Exp. Zool. A Ecol. Integr. Physiol*. 10.1002/jez.2562 (2021).
2. N. S. Baban, A. Orozaliev, S. Kirchhof, C. J. Stubbs, Y.-A. Song, *Science* **375**, 770 (2022).
3. K. Autumn *et al.*, *Proc. Natl. Acad. Sci. U.S.A.* **99**, 12252 (2002).
4. S. Gorb, Y. Jiao, M. Scherge, *J. Comp. Physiol. A* **186**, 821 (2000).
5. E. Arzt, S. Gorb, R. Spolenak, *Proc. Natl. Acad. Sci. U.S.A.* **100**, 10603 (2003).
6. M. Kappl, F. Kaveh, W. J. P. Barnes, *Bioinspir. Biomim.* **11**, 035003 (2016).
7. M. Micciché, E. Arzt, E. Kroner, *ACS Appl. Mater. Interfaces* **6**, 7076 (2014).
8. A. Ghatak, L. Mahadevan, J. Y. Chung, M. K. Chaudhury, V. Shenoy, *Proc. R. Soc. London Ser. A* **460**, 2725 (2004).
9. J. D. Gilett, V. B. Wigglesworth, *Proc. R. Soc. London Ser. B* **111**, 364 (1932).
10. E. P. Arul, A. Ghatak, *Langmuir* **25**, 611 (2009).
11. E. P. Arul, A. Ghatak, *J. Mater. Sci.* **46**, 832 (2011).
12. M. J. Vogel, P. H. Steen, *Proc. Natl. Acad. Sci. U.S.A.* **107**, 3377 (2010).
13. T. Eisner, D. J. Aneshansley, *Proc. Natl. Acad. Sci. U.S.A.* **97**, 6568 (2000).
14. T. Eisner, *For Love of Insects* (Harvard Univ. Press, 2003).
15. I. Shtein, A. Koyfman, A. Eshel, B. Bar-On, *J. R. Soc. Interface* **16**, 20180737 (2019).

10.1126/science.abn4949

Downloaded from https://www.science.org at New York University on February 18, 2022

PHOTO: RYU UCHIYAMA/WWW.MINDEN PICTURES

Science

How does a lizard shed its tail?

Animangsu Ghatak

Science, 375 (6582), • DOI: 10.1126/science.abn4949

View the article online
https://www.science.org/doi/10.1126/science.abn4949
Permissions
https://www.science.org/help/reprints-and-permissions

Downloaded from https://www.science.org at New York University on February 18, 2022

Use of think article is subject to the Terms of service

Science (ISSN 1095-9203) is published by the American Association for the Advancement of Science. 1200 New York Avenue NW, Washington, DC 20005. The title *Science* is a registered trademark of AAAS.
Copyright © 2022 The Authors, some rights reserved; exclusive licensee American Association for the Advancement of Science. No claim to original U.S. Government Works